Upper Atmospheric Planetary-Wave and Gravity-Wave Observations

C. G. JUSTUS

School of Aerospace Engineering, Georgia Institute of Technology, Atlanta 30332

ARTHUR WOODRUM

School of Physics, Georgia Southern College, Statesboro 30458

(Manuscript received 16 February 1973, in revised form 7 May 1973)

ABSTRACT

Previously collected data on atmospheric pressure, density, temperature and winds between 25 and 200 km from sources including Meteorological Rocket Network data, ROBIN falling sphere data, grenade release and pitot tube data, meteor winds, chemical release winds, satellite data, and others were analyzed by a daily-difference method, and results on the magnitude of atmospheric perturbations interpreted as gravity waves and planetary waves are presented. Traveling planetary-wave contributions in the 25–85 km range were found to have a significant height and latitudinal variation. It was found that observed gravity-wave density perturbations and wind are related to one another in the manner predicted by gravity-wave theory. It was determined that, on the average, gravity-wave energy deposition or reflection occurs at all altitudes except the 55–75 km region of the mesosphere.

1. Introduction

The variations of the upper atmosphere are due to a wide variety of sources and cover a broad range of frequencies and size scales. The shortest-period, smallest-scale variations are due to turbulence. Certain variations of only slightly longer period and larger scale are thought to be due to the action of gravity waves. There has been no unambigious resolution of gravity waves in the upper atmosphere (i.e., simultaneous observation of amplitudes, phases and frequency sufficient to verify propagation according to the theoretical dispersion equation). However, there is strong circumstantial evidence for their occurrence, and the short-period (i.e., <24 hr) irregular variations discussed in this report may be assumed to result from gravity waves.

Atmospheric tides cause variations with periods of 24 hr and harmonics (e.g., 12 and 8 hr). Longer period phenomena are the result of synoptic variations and planetary waves. Planetary waves may occur as either standing modes or traveling modes. Standing planetary-wave modes vary with longitude but their phase does not propagate with respect to an earth-fixed site. Traveling modes have both longitudinal variation and time variation with respect to a fixed location. Planetary waves have been resolved up to about 30 km (Deland and Johnson, 1968). Wind data such as presented by Finger and Teweles (1964) and Muench (1968) indicate the propagation of planetary-wave disturbances up to about 55 km and evidence for long-period waves at meteor heights has been offered (Muller, 1971). Still longer period phenomena are the seasonal, semi-annual, annual and quasi-biennial oscillations.

The analysis technique used to study gravity-wave and traveling planetary-wave variations is known as the daily-difference technique. This method was developed (Woodrum and Justus, 1968; Justus, 1970) for application to upper atmosphere data where specific removal of long-period and tidal variations would be difficult because of lack of data. This approach allows for the estimation of magnitudes and other parameters of the irregular variations of less than 1-day period. It also can be used to determine the magnitude of the variations due to traveling planetary waves of periods up to a few days.

2. Data analysis and interpretation

The daily-difference analysis technique was developed for applications where limited data did not allow explicit separation of the tidal components in order to determine the small-scale irregular variations. As an example of the application of this technique consider a vertical profile of a parameter $F(z,t)$ over height z at time t, where F may be a wind component, pressure, density or temperature. We consider that F is made up of a profile of prevailing values $F_0(z)$ which is time invariant, plus a long-period (e.g., seasonal, annual or quasi-biennial oscillation) component $S(z,t)$, a long-period traveling planetary wave or synoptically varying component $P(z,t)$, a tidal component $T(z,t)$ which may have planetary-scale wavelengths but whose periods are restricted to 24 hr and harmonics, a gravity-wave or

short-period irregular component $G(z,t)$, and a still smaller period component made up of measurement error and turbulence $E(z,t)$. Thus

$$F(z,t)=F_0(z)+S(z,t)+P(z,t)+T(z,t)+G(z,t)+E(z,t). \quad (1)$$

The component $P(z,t)$ would be composed of traveling waves only, and all truly standing waves would be included in the component $F_0(z)$ or seasonally fluctuating standing waves would be included in $S(z,t)$. The traveling-wave component, the tidal component, the gravity-wave component, and the turbulence may all have seasonally varying magnitudes, however. Two profiles of F are chosen at times t_1 and t_2 such that $t_2-t_1=\Delta t=24n$ [hr] where n is an integer. If, at any selected altitude z, the corresponding values of F are differenced, then

$$\Delta F_n(z)=F(z,t_2)-F(z,t_1)=[S(z,t_2)-S(z,t_1)]+[P(z,t_2)-P(z,t_1)]+[T(z,t_2)-T(z,t_1)]+[G(z,t_2)-G(z,t_1)]+[E(z,t_2)-E(z,t_1)]. \quad (2)$$

The following assumptions are now made:

1) The integer n is sufficiently small that $S(z,t_2)\approx S(z,t_1)$, i.e., n is a small number of days compared to times over which appreciable seasonal variation would occur. In the analysis n was restricted to 15 or less days.

2) The tidal component is diurnally repeating and Δt is a multiple of 24 hr. Hence it can be assumed that $T(z,t_2)=T(z,t_1)$. [Any systemmatic or synoptic variation in the tidal parameters would be included in the component P. Assumption 1) means that seasonal variation of the tidal parameters is negligible over the day differences n used in the analysis.]

3) The planetary-wave, gravity-wave, turbulence, and error components are uncorrelated with each other and are correlated only with themselves (autocorrelation).

Assumption 1) also means that seasonal variation of the magnitudes of planetary-wave, gravity-wave, and turbulence components is negligible over the day differences n used in the analysis. Eq. (2) can now be squared and averaged over an ensemble of different profile pairs all having the same time separation Δt. The result is

$$\langle[\Delta F_n(z)]^2\rangle=\langle[P(z,t_2)-P(z,t_1)]^2\rangle+\langle[G(z,t_2)-G(z,t_1)]^2\rangle+\langle[E(z,t_2)-E(z,t_1)]^2\rangle, \quad (3)$$

where the angle brackets denote the ensemble average process. The cross-product terms in (3) have dropped out because of assumption 3). The mean-square values of P, G and E can be considered independent of day difference n (i.e., statistically stationary) because of assumption 1) and the restriction to small day differences. If squared terms in (3) are now evaluated explicitly, then the mean-square data differences become

$$\langle[\Delta F_n(z)]^2\rangle=2\langle P^2(z)\rangle[1-\rho_P(\Delta t)]+2\langle G^2(z)\rangle\times[1-\rho_G(\Delta t)]+2\langle E^2(z)\rangle[1-\rho_E(\Delta t)], \quad (4)$$

where ρ_P, ρ_G and ρ_E are the time autocorrelation functions of P, G and E respectively.

Finally, we assume that 1) the gravity-wave, error and turbulence components are uncorrelated for all time differences of 1 day or more (i.e., $n\geqslant 1$), and 2) the planetary-wave component is of such a long period that $\rho_P(\Delta t)\approx 1$ for $\Delta t=1$ day, but for large n the planetary-wave component also becomes uncorrelated. These assumptions (and the implicit assumption that the errors are sufficiently small that meaningful results can be obtained from the analysis) are subject to verification. The results presented later in this paper indeed do confirm these assumptions (c.f., discussion of Figs. 1–5).

For single-day differences, Eq. (4) thus becomes

$$\langle[\Delta F_1(z)]^2\rangle=2[\langle G^2(z)\rangle+\langle E^2(z)\rangle], \quad (5)$$

that is, the mean-square differences in the observed data are equal to twice the mean-square magnitude of the gravity wave component plus any contribution from measurement errors or small-scale turbulence. For time separations of many days (n large, say approaching 15) and under the above assumptions Eq. (4) becomes

$$\langle[\Delta F_n(z)]^2\rangle=2[\langle P^2(z)\rangle+\langle G^2(z)\rangle+\langle E^2(z)\rangle]. \quad (6)$$

Thus, at longer time separations the magnitude of the traveling planetary-wave contributions becomes added. At intermediate time separations progressively larger portions of the traveling planetary-wave contribution [through the factor $1-\rho_P(\Delta t)$] become added. Eqs. (5) and (6) can be subtracted, yielding

$$\langle[\Delta F_n(z)]^2\rangle-\langle[\Delta F_1(z)]^2\rangle=2\langle P^2(z)\rangle. \quad (7)$$

This allows an estimate of the contribution of traveling planetary waves directly from the observed daily differences of measured data, and the estimate is unbiased with respect to the error component $\langle E^2\rangle$ since that component cancels in the subtraction process. Note, however, that this method, like any single-site method, does not resolve the standing planetary-wave components, only the traveling components.

The method outlined above can also be used to measure seasonal variations of gravity-wave and traveling planetary-wave magnitudes, as well as the effects on these magnitudes of phenomena such as solar activity and mid-winter warmings. This can be done by first dividing the data profile pairs into groups (e.g., by season, by quiet vs disturbed solar conditions, or by normal winter-time vs warming periods). Averages would then be taken separately over each group and the resultant effects would be determined from differences in the averages of each group. These analyses are pre-

sently underway and will hopefully be the subject of later reports. Preliminary results indicate no influence of solar activity on gravity waves or traveling planetary waves in the 25–65 km height region. Preliminary seasonal analysis indicates the reasonable result that gravity-wave and traveling planetary-wave magnitudes are larger in the fall and winter than in the spring and summer.

a. Structure functions

An alternate form of the correlation function known as the structure function was first used extensively by Russian meteorologists in the analysis of turbulence. The structure function of a statistically stationary, time-varying process $f(t)$ is given by

$$D(\tau)=\langle[f(t+\tau)-f(t)]^2\rangle, \quad (8)$$

where the structure function D depends only on the time displacement τ because of the statistical stationarity. The angle brackets in (8) denote averaging.

For the purpose of this paper, two properties of the structure function are important: (i) The structure function of a sinusoidal process $f(t)$ of period P is periodic with the same period P and has a first maximum value at time $\tau=P/2$. (ii) The structure function of a statistically stationary process $f(t)$ which is characterized by a correlation function $\rho(\tau)$ is given by

$$D(\tau)=2\langle f^2\rangle[1-\rho(\tau)]; \quad (9)$$

therefore, for this type of process, $D(\tau)$ approaches $2\langle f^2\rangle$ as τ approaches infinity.

Note that the daily differences discussed in the previous section are a form of structure function. For comparison with the estimations of gravity-wave magnitudes from daily difference analyses, the structure function of time-series, harmonic analysis residuals was also computed. This procedure is described next.

b. Harmonic analysis

Harmonic analysis was performed on five sets of Meteorological Rocket Network (MRN) data for the evaluation of tidal components. In the past, tidal analysis has been performed usually on data obtained from a high density of rocket launches over a basic period of about 48 hr. However, there are frequent data from single rocket launches over a period of 5–10 days before or after the basic 48 hr. A preliminary error analysis (Woodrum and Justus, 1972) indicates that the error in the harmonic analysis of the tidal components can be reduced significantly if input data include these scattered data in addition to the data of the basic 48 hr. Solar radiation corrections of the form developed by Hoxit and Henry (1972) were applied also to each data set. Then each data set was smoothed by the use of a polynomial smoothing function over 5-km height intervals. Next, a function of the following form was fitted to the smooth data by a least-squares process:

$$F(t)=A_0+A_{12}\sin(2\pi t/12+\phi_{12})+A_{24}\sin(2\pi t/24+\phi_{24}), \quad (10)$$

where time t is measured in hours, A_0 is the mean value of the parameter, A_{12} and A_{24} are the amplitudes of the 12- and 24-hr period tides, and ϕ_{12} and ϕ_{24} are phase angles for those tidal components. [The actual least-squares fit was done in terms of sine and cosine terms equivalent to (10).] The results of the harmonic analysis were subtracted from the solar-radiation-corrected data to find residual values. These residual values were evaluated at 1-km altitude increments from 25 km to 65 km. Thus, profiles of irregular variations, interpreted as gravity waves, were obtained. These gravity-wave profiles were used to compute time-structure functions according to Eq. (8), where the average was taken over all values at a given time difference from the five MRN data sets.

3. Magnitudes of gravity-wave and traveling planetary-wave variation

a. Resolution of the traveling planetary-wave component

Characteristics, probability distribution and structure of irregular winds at chemical release altitudes (~90–130 km) were first studied by Woodrum and Justus (1968) and Justus (1970). In these earlier analyses significant variations with height of the rms daily difference winds were observed. However, no variation with number of days separation between profile pairs was observed, and so, according to the concepts discussed in the previous section, it was considered that planetary waves do not propagate to the 90–130 km level with sufficient amplitude to be detectable.

A large number of data in the 25–200 km height range from various sources were collected for analysis by the daily difference method. These data included Meteorological Rocket Network, grenade, pitot tube, falling sphere, meteor winds, and satellite measurements as well as chemical release data. A complete list of data sources and references was provided in earlier reports of this study (Justus and Woodrum, 1972, 1973).

Mean-square daily differences were computed separately for each day of separation in order to determine if traveling planetary-wave contributions could be detected. The results are shown in Figs. 1–5. These figures show the mean-square daily differences in the 25–45 km and 45–65 km regions, as a function of the number of days separation from 1 to 15 days.

At the earlier times (1–72 hr) in Figs. 1–5, time-structure functions of the residual winds and thermodynamic variables from the harmonic analysis are plotted. These data together with the daily-difference

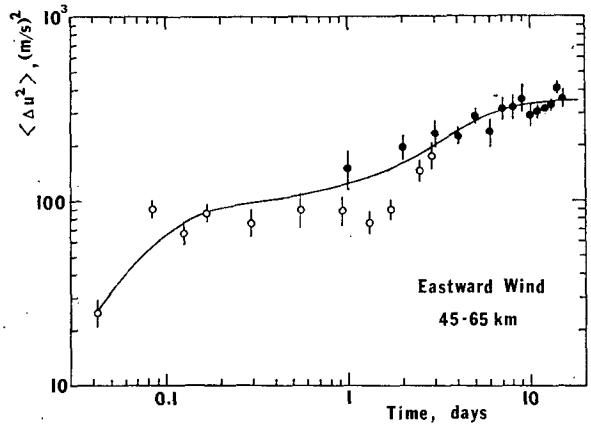

FIG. 1. Time structure function of gravity-wave and traveling planetary-wave eastward wind component over the range from 1 hr to 15 days over the height interval 45–65 km. Solid dots are from daily-difference analysis and open circles from residuals after removal of tides determined by least-squares harmonic analysis of time-series data.

results can be interpreted as a continuous-valued structure function of the gravity-wave and traveling planetary-wave components. The time-structure data from the residual winds of the tidal analysis represent an average over five sets of data made up of from 22–35 profiles in each set spread over a time span of 10–20 days, with from 13–24 profiles occurring in a basic 48-hr interval for each set.

A distinct peak at a time lag of 3 hr (corresponding to a wave period of 6 hr) was found in the density, temperature and pressure structure functions in both the 25–45 km and 45–65 km height ranges. Possibly this indicates a preferred gravity-wave period of 6 hr during the time from which data were available. No corresponding peak at 3 hr in the structure function of the gravity-wave winds was found with the exception of the northward component winds in the 25–45 km height range (Fig. 2). It should be noted that the 6-hr period peak was not found in time-structure functions

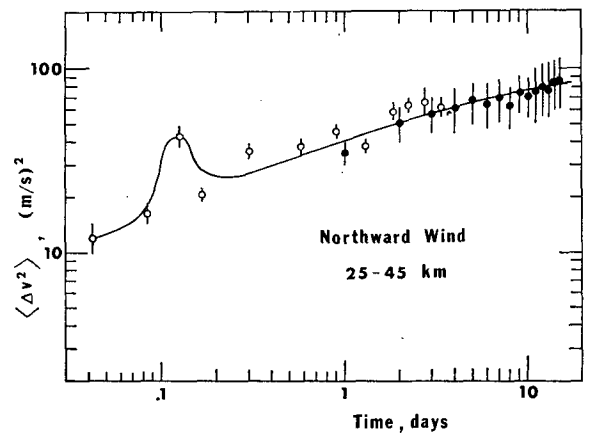

FIG. 2. As in Fig. 1 except for northward wind component over 25–45 km.

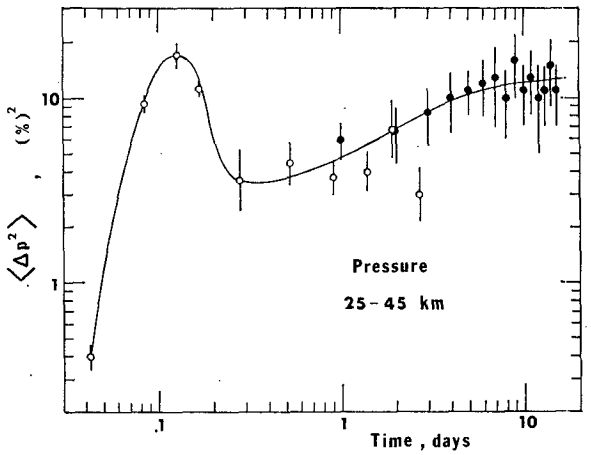

FIG. 3. As in Fig. 1 except for pressure over 25–45 km.

computed from residual winds from non-solar-corrected data. Hence the possibility exists that the 6-hr period peak is due to extraneous 6-hr period variance introduced by the solar correction process.

The time-structure functions at 1 hr are definitely smaller than those at subsequent times and can be taken as an indication of the upper limit ϵ of the contribution from error and small-scale turbulence. This rms upper limit ϵ is related to the structure function at 1 hr by $\epsilon=[D(1)/2]^{\frac{1}{2}}$. This relation results in the following estimate for the upper limits of error in the 45–65 km height range: 1% for pressure and density, 0.8% for temperature (~2K), and 3.5–4.7 m sec^{-1} for wind. These estimates are only slightly smaller than those computed by Avera and Miers (1971) for this height region. Their estimates were 2.6K for temperature and 6.5 m sec^{-1} for wind.

The daily-difference structure functions in Figs. 1–5 are reasonably continuous with the structure functions of the harmonic analysis residuals, considering the smaller amount of data available for the harmonic analysis and the large amount of data in the daily differences. The daily differences in Figs. 1–5 are

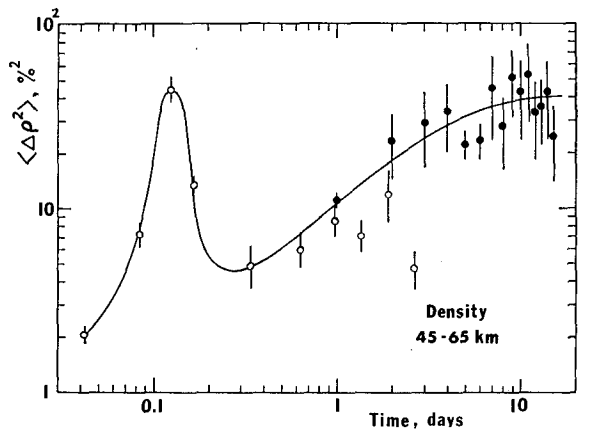

FIG. 4. As in Fig. 1 except for density over 45–65 km.

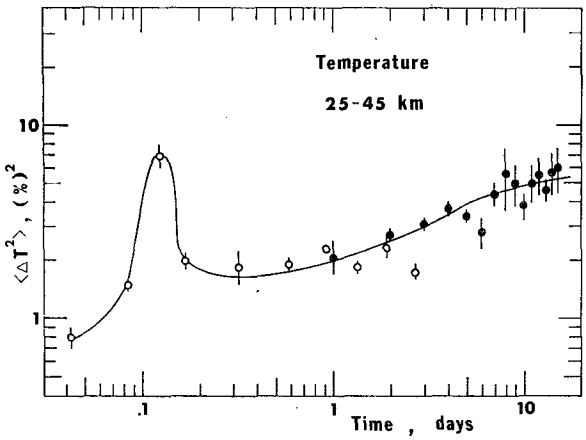

FIG. 5. As in Fig. 1 except for temperature over 25–45 km.

averaged over three MRN sites (Ascension Island, Cape Kennedy and Fort Greely) and over altitudes from either 25–45 km or from 45–65 km with data from 1964 through 1969. The daily-difference magnitudes definitely increase with time separation and it appears that the daily differences at 1-day separation may be used as a reasonable estimate of the gravity-wave contribution because of their general agreement with the values of the gravity-wave structure functions at time scales larger than 5 hr (i.e., periods >10 hr). Since, the daily-difference magnitudes are fairly uniform over 7–15 day time separations, an average over this interval can reasonably be taken as a measure of the combined gravity-wave and traveling planetary-wave (up to 30 day period) contributions.

Traveling planetary-wave magnitudes were extracted from the 7–15 day time separation data for each of the three MRN sites mentioned above by the method described by Eq. (7), except that instead of one daily difference at large day number n, an average of the daily differences between 7 and 15 days was used. The results are presented in Fig. 6. Primary contributions to the traveling planetary-wave magnitudes of Fig. 6 would come from the period range 14–30 days. Data points represent averages over 10-km altitude sections centered about the point. The data of Fig. 6 represent low, middle and high latitudes with results from Ascension Island (8S), Cape Kennedy (28.5N) and Fort Greely (64N). The east-west traveling planetary-wave wind component magnitude is larger than the north-south component magnitude except at the high-latitude site. Significant latitude variation in the 25–65 km altitude region was found. A steady increase in traveling planetary-wave magnitude with increasing latitude was observed for the pressure, density, temperature, and northward velocity component. The eastward component was reasonably similar at all latitudes.

Above 65 km there were insufficient data for analysis of separate sites and so all data were combined for

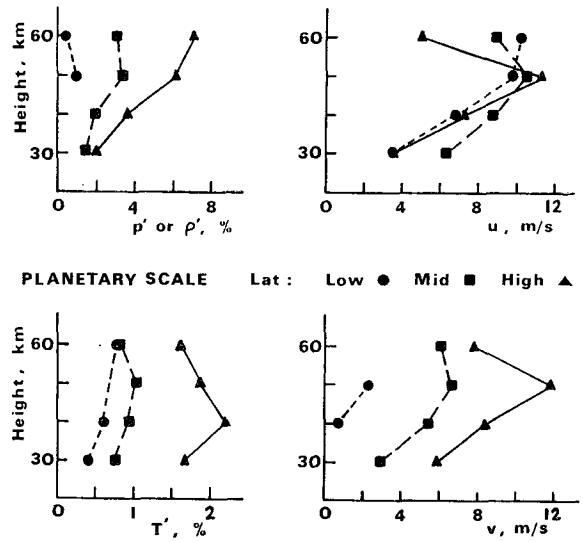

FIG. 6. Height and latitude variation of the traveling planetary-wave component. The solid dots are Ascension Island data (8S), the squares Cape Kennedy (28.5N), and the triangles Fort Greely (64N).

averaging. In the 65–85 km region and above it was found that the daily differences at 7–15 days time separation were not significantly larger than 1-day differences, which indicates no measurable propagation of planetary waves to this altitude range. However, from analysis of vertical scales (Justus and Woodrum, 1972,

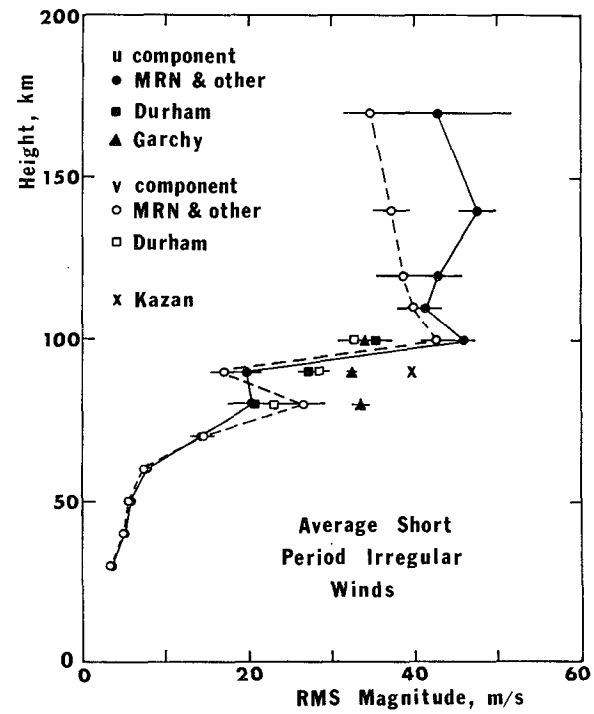

FIG. 7. Height variation of the magnitude of gravity-wave wind components. The eastward component is u and the northward component v.

TABLE 1. MRN site locations.

Site	Latitude	Longitude
Ascension Island, A.F.B.	7°59′S	14°25′W
Fort Sherman, Canal Zone	9°20′N	79°59′W
Barking Sands, Hawaii	22°02′N	159°47′W
Cape Kennedy, Fla.	28°27′N	80°32′W
White Sands, N. M.	32°23′N	106°29′W
Point Mugu, Calif.	34°23′N	119°07′W
Fort Churchill, Canada	58°44′N	93°49′W
Fort Greely, Alaska	64°00′N	145°44′W

1973) there is evidence for propagation of selected wavelengths of traveling planetary waves into the 65–85 km region.

b. Gravity-wave magnitudes

The daily differences over 1-day separation were used to compute gravity-wave magnitudes in the 25–85 km region. Because planetary-scale waves were not detectable in the 95–110 km region (Justus, 1970) data determined from averages over 1–15 day separation daily differences were used as the best estimates of gravity wave magnitudes above 85 km.

Fig. 7 shows the height variation of the measured average gravity-wave magnitude. The data in Fig. 7 were obtained from 1964–69 MRN data daily differences from all eight sites listed in Table 1 plus all of the other falling sphere, grenade, pitot tube, chemical release, and satellite data collected. One-day differences only were used in the 25–85 km height range and 1–15 day differences were used above 85 km. Meteor wind data from Garchy, France (Spizzichino[1]; Spizzichino and Revah, 1967), Durham, N. H. (Barnes[1]; Barnes and Pazniokas, 1972), and Kazan, Russia (Pokrovskiy *et al.*, 1969) are shown separately in Fig. 7. These meteor wind results are residual winds after explicit resolution of the tidal winds by the method of Groves (1959). The error bars in Fig. 7 were computed by the method outlined in Appendix A.

The meteor wind results agree qualitatively although not in detail with the average results from the other data. However, it should be noted that the meteor results from Garchy and Durham were each determined from one set of measurements over a few days whereas the other results were obtained from several profile pairs from times spread over several years.

The two gravity-wave velocity components appear to be isotropic over the full altitude extent of Fig. 7 with the possible exception of a slight predominance of the eastward component near 140 km.

Linearized gravity-wave theory (Hines, 1960) with no dissipation or reflection predicts that the gravity-wave kinetic energy density $\rho_0\langle u^2+v^2\rangle$ remains constant with height. However, Fig. 8 shows that considerable dissipation and/or reflection takes place, on the average, throughout most of the atmosphere. One exception is the 55–75 km height region, which corresponds to the decreasing temperature gradient of the mesosphere, a region where gravity wave reflection is not expected. At 90 km in Fig. 8 the solid dot represents the MRN and other data and the open circle represents an average value including the meteor wind data. Between 75 and 135 km the average gravity-wave kinetic-energy density varies with height as

$$\rho_0\langle u^2+v^2\rangle \propto \exp(-z/z_0), \tag{11}$$

where the "scale height" value z_0 is 7.8 km, in good agreement with the value determined by Kochanski (1964) in the upper portion of this altitude range. Between 25 and 55 km the value for z_0 is 9.4 km. Extrapolation of $\rho_0\langle u^2+v^2\rangle$ to 10 km indicates that jet-stream-level perturbations of about 3 m sec^{-1} would be required to maintain the same rate of dissipation or reflective loss between 10 and 30 km as that observed between 30 and 50 km. If tropospheric propagation from the surface to 10 km is assumed to be at constant energy, analogous to the mesospheric propagation, then surface perturbations of about 1.8 m sec^{-1} could maintain the dissipation or reflective loss of the extrapolated curve. The change of slope above 135 km is due to a change in the density variation at this altitude, while the gravity-wave wind magnitude remains approximately constant with height.

The height variation of the gravity-wave pressure, density and temperature is shown in Fig. 9. The data are expressed as variations relative to the mean atmospheric parameters. Error bars in Fig. 9 were also computed by the method outlined in Appendix A. Fig. 9 shows that the relative temperature variation magnitude between 40 and 70 km is significantly smaller

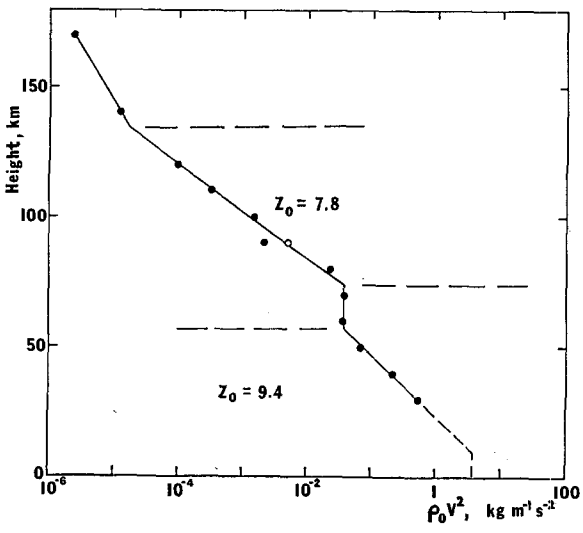

FIG. 8. Height variation of the kinetic energy density of gravity-wave winds. Z_0 values are energy "scale height" values for Eq. (11). The solid dots are the MRN and other data. The open circle at 90 km is an average value including meteor wind data.

[1] Personal communications, 1971.

than for the relative pressure or density, which are about equal. Between 80 and 100 km the relative pressure and temperature variation magnitudes become about equal and smaller than the relative density variations. Above 100 km the relative density variations become smaller than those for the relative temperature.

At first one might think that the Boussinesq approximation should apply to the pressure, density and temperature variations and hence that the relative pressure variations should be much smaller than the relative density and temperature. However, as shown by Dutton and Fichtl (1969), for motions of vertical scale not small compared to the scale height, the magnitudes of all three parameters are comparable. It was found (Justus and Woodrum, 1972, 1973) that the vertical scales are comparable with the scale height. Therefore, the relative values of the irregular thermodynamic parameters are related by

$$p'/p_0=\rho'/\rho_0+T'/T_0, \tag{12}$$

and in the mean square they would be related by

$$\langle(p'/p_0)^2\rangle=\langle(\rho'/\rho_0)^2\rangle+\langle(T'/T_0)^2\rangle +2\langle(\rho'/\rho_0)(T'/T_0)\rangle, \tag{13}$$

where the last term is basically the correlation between the density and temperature variations, which would be dependent on the relative phase between the density and temperature wave variation. The changes discussed above in the relative magnitudes of the thermodynamic variable of Fig. 9 therefore indicate a changing phase relationship with height. This changing phase relationship could result from the action of viscosity or conductive losses, from nonlinear interactions between gravity-wave modes, or by selective absorption or reflection of modes which leave the remaining modes with a different effective phase difference between density and temperature variation.

On initial consideration it seems unreasonable that the gravity-wave density and temperature magnitudes in Fig. 9 should decrease considerably at heights above 100 km while the gravity-wave winds of Fig. 7 are relatively constant above 100 km. However, this phenomenon can be explained by gravity-wave theory. Isothermal non-dissipative gravity-wave theory (Hines, 1960) predicts that for low-frequency gravity waves the density amplitudes $|\rho'/\rho_0|$ are related to wind amplitudes $\langle u^2+v^2\rangle$ by

$$|\rho'/\rho_0|=\{[(\gamma-1)c^2]\langle u^2+v^2\rangle\}^{\frac{1}{2}}, \tag{14}$$

where γ is the ratio of specific heats and c the speed of sound. Miller (1971) has generalized this equation for non-isothermal conditions. His form of (14) is

$$|\rho'/\rho_0|=\{[(\gamma-1)/c^2+(1/gT_0)dT_0/dz]\langle u^2+v^2\rangle\}^{\frac{1}{2}}, \tag{15}$$

where g is the acceleration of gravity and T_0 the mean temperature. To evaluate (14) and (15), 1962 U. S. Standard Atmosphere values were used for the speed

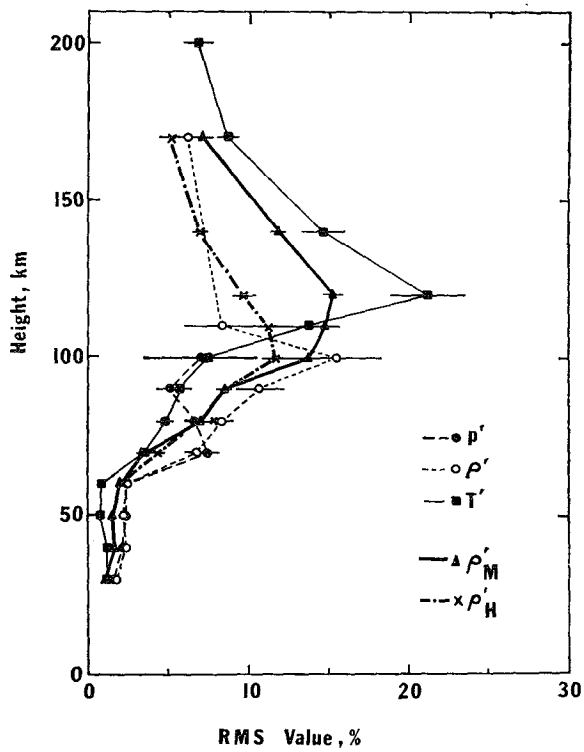

FIG. 9. Height variation of the magnitude of the relative pressure p'/p_0 (30–100 km only), density ρ'/ρ_0, and temperature T'/T_0 due to gravity waves, and the density perturbation magnitudes computed from observed gravity-wave winds (from Fig. 7). Values computed from Eq. (14) are indicated ρ_H' and values from Eq. (15) by ρ_M'.

of sound c, the acceleration of gravity g, the temperature T_0, and its height gradient dT_0/dz; the ratio of specific heats γ was assumed to be constant at a value of 1.4; and observed winds were taken from Fig. 7. Values computed from Eq. (14) are shown as curve ρ_H' in Fig. 9 and values computed from Eq. (15) are shown as curve ρ_M'. The two curves ρ_H' and ρ_M' are essentially equal below 100 km, but the effects of the dT_0/dz term in (15) become important above that height. Both curves indicate that the decreasing ρ'/ρ_0 magnitude above 100 km is to be expected from the theoretical coefficient relating gravity-wave density amplitudes to wind amplitudes. The isothermal equation (14) actually fits the observed ρ'/ρ_0 data better above 100 km. The agreement between the observed ρ'/ρ_0 variation and that predicted by the theoretical formula and observed winds is remarkably good, considering the uncertainties introduced by the use of standard atmosphere values and the application of non-dissipative, single-mode, gravity-wave theory to a field of gravity waves which probably satisfies neither of these assumptions.

The three sites, Ascension Island, Cape Kennedy and Fort Greely, had sufficient data for daily differences over 1-day separation so that separate evaluations could be made for these sites. Fig. 10 shows the altitude

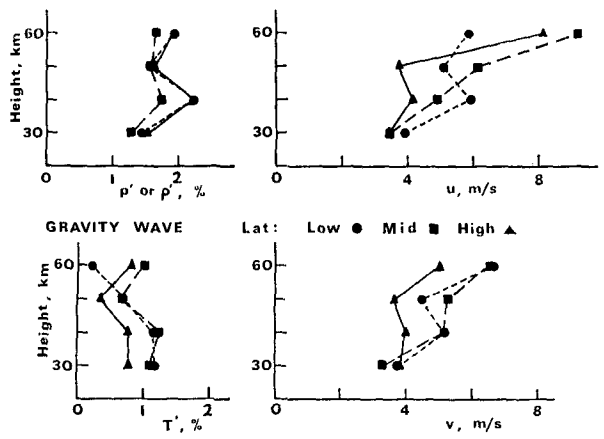

FIG. 10. Height and latitude variation of the gravity-wave component. Ascension Island data are shown by the solid dots, Cape Kennedy by the squares, and Fort Greely by the triangles.

variation of the rms gravity-wave magnitudes at these locations. There is no apparent system which describes the variation with latitude at all altitudes, although at many heights the magnitudes of wind and temperature fluctuations are smaller for the Fort Greely site. The large increase in wind magnitude between 50 and 60 km is compatible with the constant kinetic energy in this region, as discussed previously.

4. Conclusions

It is concluded that the daily-difference technique can be used to derive information on gravity-wave and traveling planetary-wave disturbances above 25 km. The height and latitude variation of traveling planetary waves in the 25–85 km range was determined. These waves were found generally to increase in magnitude with increasing latitude. It was inferred from vertical scale studies reported elsewhere (Justus and Woodrum, 1972) that only selected wavelengths of planetary waves propagate to the 65–85 km height region. Therefore, the maximum planetary-wave amplitudes probably occur between about 50 and 60 km (see Fig. 6).

Gravity waves propagate upward but with considerable damping or reflective losses except in the 55–75 km height region. One likely result of these upward energy losses is the production of turbulence by nonlinear energy deposition or critical layer development. Gravity-wave theory was found to relate the observed gravity-wave density perturbation magnitude to the observed gravity-wave wind magnitude reasonably well considering the approximations involved in both the theory and in the use of standard atmosphere values for evaluation of certain terms in the equations.

Acknowledgments. The analysis work above 50 km was supported by NASA Contract NAS8-26658. The analysis of data in the 25–50 km altitude range was supported by NASA Grant NGL-11-002-004, with Dr. H. D. Edwards of Georgia Tech as project director.

Our thanks go to many people who have supplied us with data and information: to Mr. Dale Johnson of NASA Huntsville who sent us the MRN data for 1964–68 on magnetic tape, to Mr. Robert W. Lenhard of AFCRL who was instrumental in our obtaining magnetic tapes of the ARCAS–ROBIN data, to Dr. Arnold A. Barnes of AFCRL and Dr. A. Spizzichino who supplied Dr. R. G. Roper of Georgia Tech with the meteor wind data from Durham, N. H., and Garchy, France, to Dr. Roper who performed the Groves analysis of the meteor data, to Dr. John Theon of NASA Goddard who sent us the collected reports of their grenade release results, and to Mr. J. F. Bedinger of GCA and Dr. N. W. Rosenberg of AFCRL who supplied us with reports and other data on chemical release winds.

APPENDIX

Error Estimate in Standard Deviation from Measured Fourth Moments

Consider a set of values x_i, $i=1$–N, which have mean zero ($\bar{x}=\langle x\rangle=0$) and standard deviation $\sigma(\langle x^2\rangle=\sigma^2)$. We now wish to compute an estimate of the error ϵ_σ in the measured value of σ. The variance of the set of data values is $v=\langle x^2\rangle$ and the individual contributions to the variance are $v_i=x_i^2$. The standard deviation S of the variance values is given by

$$S^2=\langle(v_i-\bar{v})^2\rangle=\langle v^2\rangle-\bar{v}^2, \tag{A1}$$

and the error ϵ_v in the mean variance estimate can be taken as

$$\epsilon_v^2=(\langle v^2\rangle-\bar{v}^2)/(N-1), \tag{A2}$$

where N is the number of independent values in the total of n values of x. Since $\bar{v}=\sigma^2$ and $\langle v^2\rangle=\langle x^4\rangle=\beta\sigma^4$, where β is the kurtosis of the x distribution (i.e., $\beta=\langle x^4\rangle/\sigma^4$), then (A2) becomes

$$\epsilon_v^2=\sigma^4(\beta-1)/(N-1). \tag{A3}$$

Now the error ϵ_σ in the mean σ value is related to ϵ_v by

$$(\sigma\pm\epsilon_\sigma)^2=\bar{v}\pm\epsilon_v, \tag{A4}$$

but, from expansion of the left side of (A4),

$$(\sigma\pm\epsilon_\sigma)^2\approx\sigma^2\pm2\epsilon_\sigma\sigma, \tag{A5}$$

where the second-order term in ϵ_σ has been neglected. Since $\bar{v}=\sigma^2$, then it is apparent from combination of (A4), (A5) and (A3) that

$$\epsilon_\sigma\approx\epsilon_v/2\sigma=(\sigma/2)[(\beta-1)/(N-1)]^{\frac{1}{2}}. \tag{A6}$$

The use of the divisor $N-1$ in (A2) means that the error is of the nature of an error of the mean. Thus, ϵ_σ from (A6) gives an error which would represent the range of deviation of the mean values of σ obtained from comparable data sets each made up of N independent values.

The number of independent daily difference data values are less than the total number for two reasons: 1) data values at adjacent heights are not independent, but are correlated with each other; and 2) if a set of data from k consecutive days are to be analyzed by the daily-difference method, then $k(k-1)/2$ differences can be formed but only $k-1$ of these differences are independent of each other. To account for the correlation over height, it was assumed that data values separated by 5 km of altitude could be taken as independent for purposes of computing the number of independent observations N.

REFERENCES

Avera, E. P., and B. T. Miers, 1971: The noise characteristics of selected wind and temperature data from 30–65 km. Tech. Rept. ECOM-5402, White Sands Missile Range, N. M.

Barnes, A. A., and J. J. Pazniokas, 1972: Results from the AFCRL radar meteor set. AFCRL-72-0185.

Deland, R. J., and K. W. Johnson, 1968: A statistical study of the vertical structure of travelling planetary scale waves. *Mon. Wea. Rev.*, **96**, 12–22.

Dutton, J. A., and G. H. Fichtl, 1969: Approximate equations of motion from gases and liquids. *J. Atmos. Sci.*, **26**, 241–254.

Finger, F. G., and S. Teweles, 1964: The mid-winter warming and circulation change. *J. Appl. Meteor.*, **3**, 1–15.

Groves, G. V., 1959: A theory for determining upper atmospheric winds from radio observations on meteor trails. *J. Atmos. Terr. Phys.*, **16**, 344–356.

Hines, C. O., 1960: Internal atmospheric gravity waves at ionospheric heights. *Can. J. Phys.*, **38**, 1441–1481.

Hoxit, L. R., and R. M. Henry, 1972: Diurnal and annual temperature variations in the 30–60 km region as indicated by statistical analysis of rocketsonde temperature data. Paper presented at Intern. Conf. Aerospace and Aeronautical Meteorology, Washington, D. C.

Justus, C. G., 1970: Distribution and structure of irregular winds near 100 kilometers. *J. Geophys. Res.*, **75**, 2171–2178.

——, and Arthur Woodrum, 1972: Atmospheric pressure, density, temperature, and wind variations between 50 and 200 km. NASA CR-2062.

——, and ——, 1973: Short and long period atmospheric variations between 25 and 200 km. NASA CR-2203.

Kochanski, A., 1964: Atmospheric motions from sodium cloud drifts. *J. Geophys. Res.*, **69**, 3651–3662.

Miller, E. B., 1971: Atmospheric density variations related to internal gravity waves. NASA CR-61359.

Muench, H. S., 1968: Large-scale disturbances in the summertime stratosphere. *J. Atmos. Sci.*, **25**, 1108–1115.

Muller, H. G., 1971: How the wind blows. *Nature Phys. Sci.*, **230**, 181–182.

Pokrovskiy, G. B., V. M. Starostin and G. M. Teptin, 1969: The distribution of turbulent wind velocities in the meteoric region of the atmosphere. *Izv. Atmos. Ocean Phys.*, **5**, 631–635.

Spizzichino, A., and J. Revah, 1967: Nouvelles données experimentales sur les differentes composantes du vent au moyer d'un radar météorique et discussion des resultats obtenus aus moyen de fusées. *Space Research VIII*, Amsterdam, North Holland Publ. Co., 679–682.

Woodrum, Arthur, and C. G. Justus, 1968: Measurement of the irregular winds in the altitude region near 100 kilometers. *J. Geophys. Res.*, **73**, 7535–7537.

——, and ——, 1972: Tidal variations of wind components and thermodynamic variables in the 45 to 60 km height range. Paper presented at the American Geophysical Union Meeting, Washington, D. C.